ORIGINAL PAPER

Deterministic and probabilistic analysis of a multi-sliding zone reservoir bank landslide influenced by the combined effects of reservoir water level fluctuation and precipitation

Wengang Zhang[1,3] · Xiangrong He[1] · Luqi Wang[1,2,3] · Xuanyu Meng[1] · Songlin Liu[1]

Abstract

Landslides represent a prevalent geological hazard in reservoir areas, posing significant risks to the lives and properties of residents. It is widely acknowledged that rainfall and the fluctuation of reservoir water level are two primary factors triggering reservoir landslides. However, there has been limited research on multi-sliding zone reservoir bank landslides, and existing studies fail to adequately characterize the evolutionary process of this type of landslide. In this paper, the Outang landslide located in Three Gorges Reservoir (TGR) was taken as a case study to evaluate its stability and failure probability. Sensitivity analyses were conducted on statistical mechanical parameters and autocorrelation functions initially, followed by a comparative analysis of annual stability and reliability. The results indicate that the stability of the Outang landslide is predominantly influenced by the water level fluctuation, and the lower sliding zone plays a pivotal role in affecting the overall stability compared with other regions in the landslide. Furthermore, variations in failure probability are notably influenced by the frictional angle and the vertical scale of fluctuation, with autocorrelation functions playing a more significant role when the coefficient of variation is small and the vertical scale of fluctuation is large. This study could provide valuable guidance for the prevention and mitigation of analogous multi-sliding zone reservoir bank landslides.

Keywords Rainfall · Reservoir water level · Sensitivity analysis · Slope stability · Reliability evaluation

Introduction

The Three Gorges Project is of immense scale and ranks among the world's largest hydraulic engineering projects. It plays a significant role in hydroelectric power generation and flood control (Sun et al. 2016; Wang et al. 2024). Nevertheless, the geological structure of the Three Gorges Reservoir (TGR) is highly intricate, with landslides being extensively distributed (Deng et al. 2023; Huang et al. 2017; McKay et al. 1979). It has been reported that, since the impoundment of the TGR in 2003, over 140 sections of both unstable and stable reservoir banks have been identified, and more than 5,000 landslides of various sizes have been documented (Huang et al. 2020b; Wang 2021; Wu et al. 2017). The instability of landslides poses catastrophic risks to the lives and properties of the local population. Therefore, comprehensively understanding the destabilization mechanisms of landslides and accurately assessing their stability is a crucial step toward mitigating geological hazards in the reservoir area.

It has been widely accepted that reservoir water level fluctuation and rainfall are the two main triggering factors of reservoir bank landslides (Chen et al. 2018; He et al. 2016; Zhang et al. 2020a). For example, the Baishuihe landslide (Li et al. 2010; Miao et al. 2021), the Qianjiangping landslide (Jian et al. 2014; Jiao et al. 2014), and the Bazimen landslide (Tu et al. 2011; Zhou et al. 2016) were induced by the coupling influence of rainfall and reservoir water level fluctuation. The abrupt and substantial increase of reservoir level could change the water content of the slope, then softening the slip zone and reducing the slip resistance of the

✉ Luqi Wang
   wlq93@cqu.edu.cn

1   School of Civil Engineering, Chongqing University,
    Chongqing 400045, China

2   State Key Laboratory of Geohazard Prevention
    and Geoenvironment Protection, Chengdu University
    of Technology, Chengdu 610059, China

3   Chongqing Field Scientific Observation Station for Landslide
    Hazards in Three Gorges Reservoir Area, Chongqing
    University, Chongqing 400045, China

slope (Zeng et al. 2023; Zhang et al. 2024). Likewise, the sudden drawdown of reservoir level will lead to significant changes in the seepage field within the slope, creating high seepage pressure pointing outward, which is critically detrimental to the stability of the slope (Chen et al. 2021; Jiang et al. 2011; Wang et al. 2023; Zhang et al. 2020a). Rainfall also directly affects the stability of the reservoir bank slope, the continuous infiltration of rainfall saturates the cracks at the rear of the slope, resulting in increased sliding force. Additionally, intense rainfall can trigger overall slope failure due to scouring and eroding the surface soil (Chen et al. 2018; Li et al. 2015; Wang and Zhang 2021).

Due to variations in mineral composition, depositional environment, stress paths, and other geological factors, the properties of geotechnical parameters exhibit spatial variability. The theory of random fields provides an effective means to characterize spatial variability, and research on random fields has made continuous advancements, ranging from one-dimensional to multi-dimensional analysis and from isotropic to anisotropic conditions (Ching et al. 2011; Griffiths and Fenton 2004; Ma et al. 2024; Salgado and Kim 2014). Studies have demonstrated that deterministic analysis without considering spatial variability significantly deviates from reality (Gu et al. 2022; Xue et al. 2020; Zhang et al. 2020b). Therefore, it is imperative to accurately quantify and consider the impact of spatial variability in geotechnical parameter analysis while evaluating slope stability (Jiang et al. 2022; Liu et al. 2017).

There has been limited research on multi-sliding zone reservoir bank landslides, and the reliability evaluation of this type of landslide is still missing. Therefore, in order to comprehensively understand the impact of reservoir water level fluctuation and rainfall on the annual stability of the landslide, as well as the relative role of these dual factors in triggering the landslide, the Outang landslide, a typical case of multi-sliding zone reservoir bank landslide in the TGR, was selected as a research case. Subsequently, based on the actual reservoir water level fluctuation and rainfall in 2014, sensitivity analysis was undertaken in this study to assess the influential factors affecting the failure probability, then the deterministic and probabilistic stability analysis of the Outang landslide within one year was evaluated (a flow chart of deterministic and probabilistic analysis of the Outang landslide is shown in Fig. 1).

Study area

Location and hydrogeological conditions

The Outang landslide is located in Anping Town, Fengjie County, Chongqing Municipality, China (109°21′15″E, 30°57′45″N), on the southern bank of the Yangtze River (Fig. 2). It is 12 km away from Fengjie county and 177 km away from the Three Gorges Dam. Outang landslide area is characterized by shallow medium-cut monoclinic low mountain valley landforms, and the planar morphology of the landslide exhibits an oblique and inverted ancient bell shape. The elevation of the landslide toe and crown is 95 m and 705 m, respectively, thus, the altitude difference of the landslide is approximately 610 m. It is estimated that the landslide is of about 1990 m in length, 890 m in width, covering an area of 176.9×10^4 m^2 and with a volume of 8950×10^4 m^3. The landslide is classified as an extremely large bedding rock landslide, with a main slip direction of 345°. The overlying strata in the landslide area are mainly composed of Quaternary residual and colluvial deposits (Q_4^{dl+el}), alluvial and diluvial deposits (Q^{al+pl}), landslide deposits (Q_4^{del}), and the Lower Jurassic Zhenzhuchong Formation (J_1z). The geomechanical properties of the soil and rock in this region display substantial variations, while the structural composition is characterized by a high degree of complexity. After a detailed investigation of the Outang landslide, this ancient instability was characterized by multi-stages and multi-period sliding, hence, it could be divided into three reactivated sliding masses (Fig. 3), sliding mass S1 (subzone I), S2 (subzone II), and S3 (subzone III). As illustrated in Fig. 4, three weak interlayers (WI 1, WI 2, WI 3) were identified. Sliding mass S1 is of about 880 m in length, 1100 m in width, covering an area of 92.2×10^4 m^2, sliding mass S2 is about 440 m in length, 650 m in width, covering an area of 31.6×10^4 m^2 while sliding mass S3 extends around 640 m in length, 830 m in width, covering an area of 54.3×10^4 m^2. The rear part of the sliding masses S1 and S2 were covered by S2 and S3, respectively.

The Outang landslide area falls within the subtropical warm-temperate monsoon climate zone, characterized by distinct seasons and features such as limited sunshine, high humidity, abundant rainfall during autumn and summer, and frequent fog during winter and spring. Approximately 70% of the annual precipitation is concentrated between the months of May and September, the maximum annual rainfall reaches 1636.3 mm, with a peak monthly rainfall of 548.4 mm and a maximum daily rainfall of 158.6 mm, these values indicate a pronounced concentration of rainfall distribution. In order to meet the requirements of power generation and flood control in the TGR, the reservoir water level fluctuates periodically between 145 and 175 m, abundant rainfall and periodic reservoir water level fluctuations are crucial external dynamic factors that significantly contribute to slope deformation and failure.

Deformation characteristics of the Outang landslide

Outang landslide is an ancient, giant, bedding landslide that has shown significant deformation in recent years. According to incomplete statistics, over 160 cracks of various
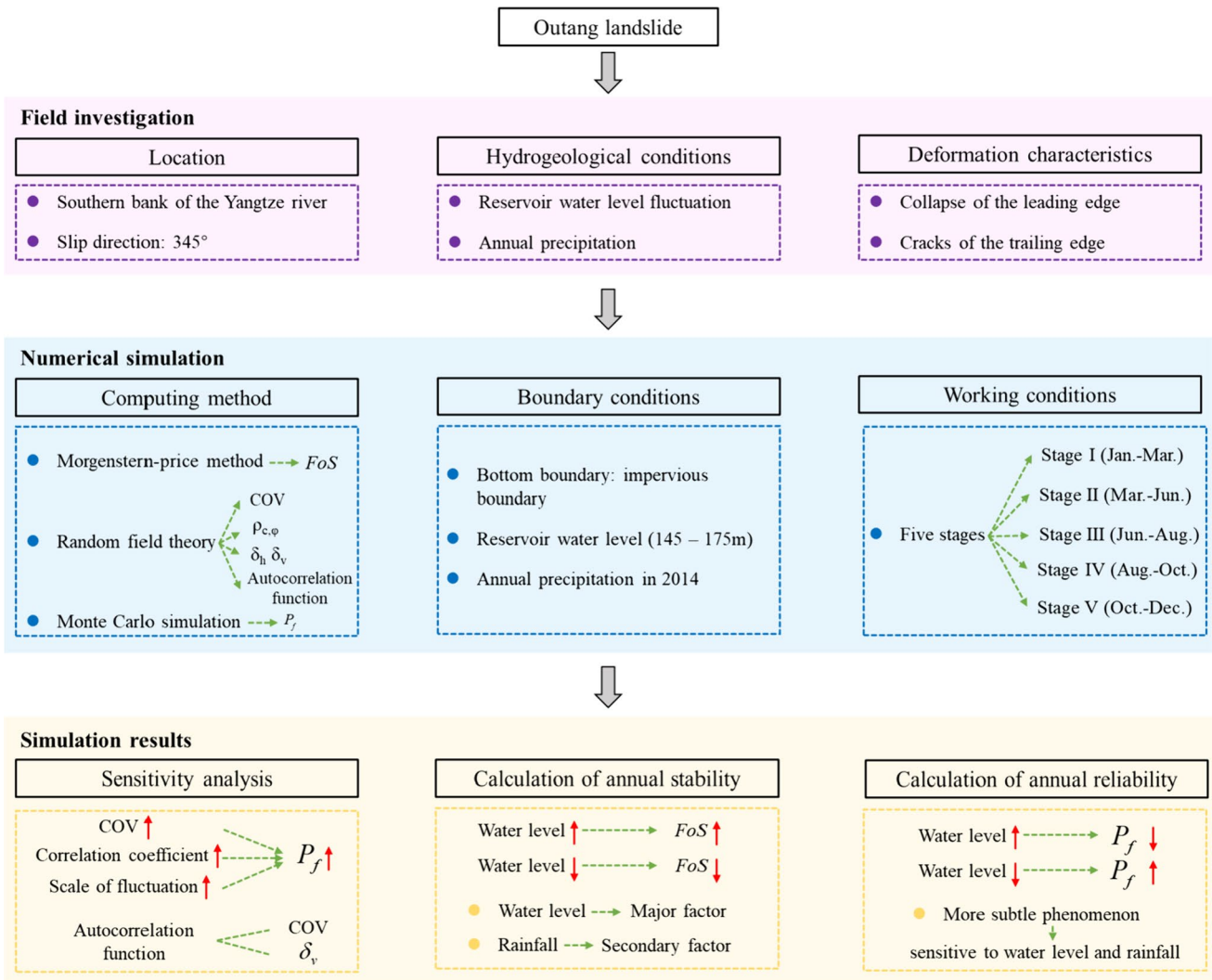
Fig. 1 Flow chart of deterministic and probabilistic analysis of the Outang landslide
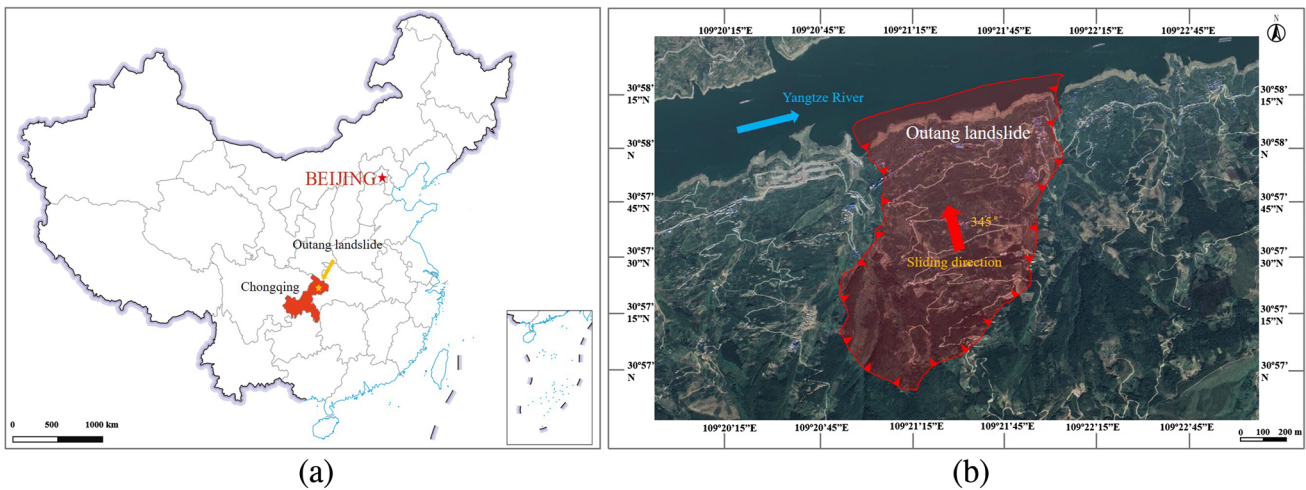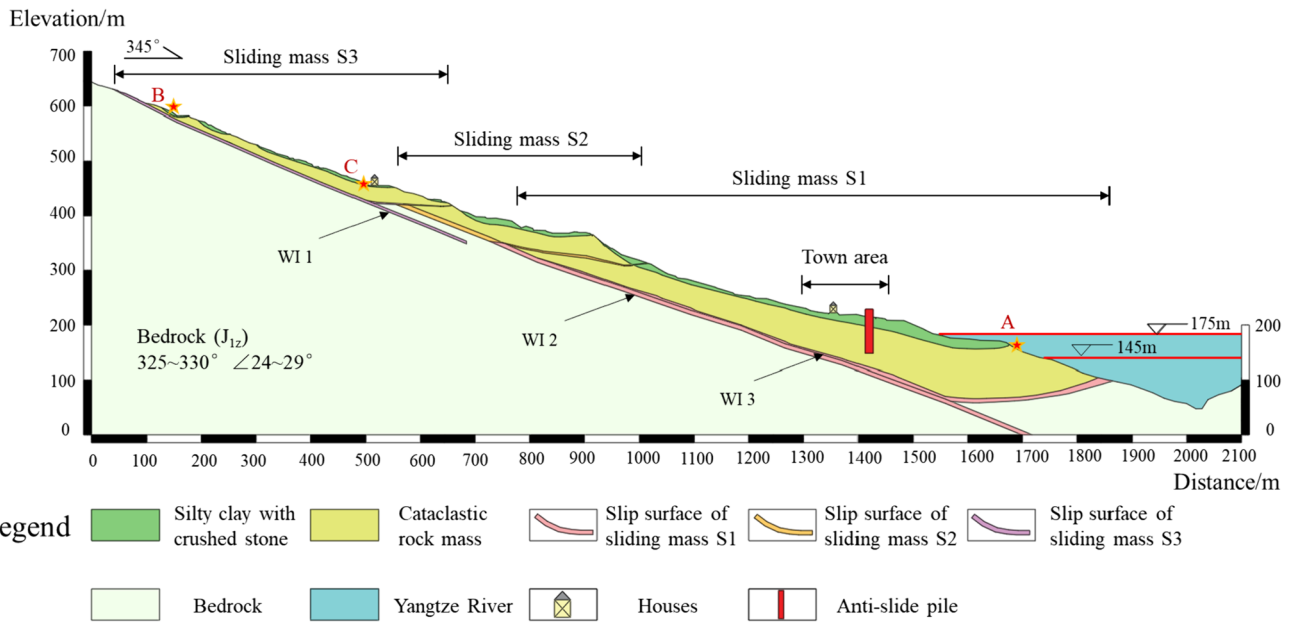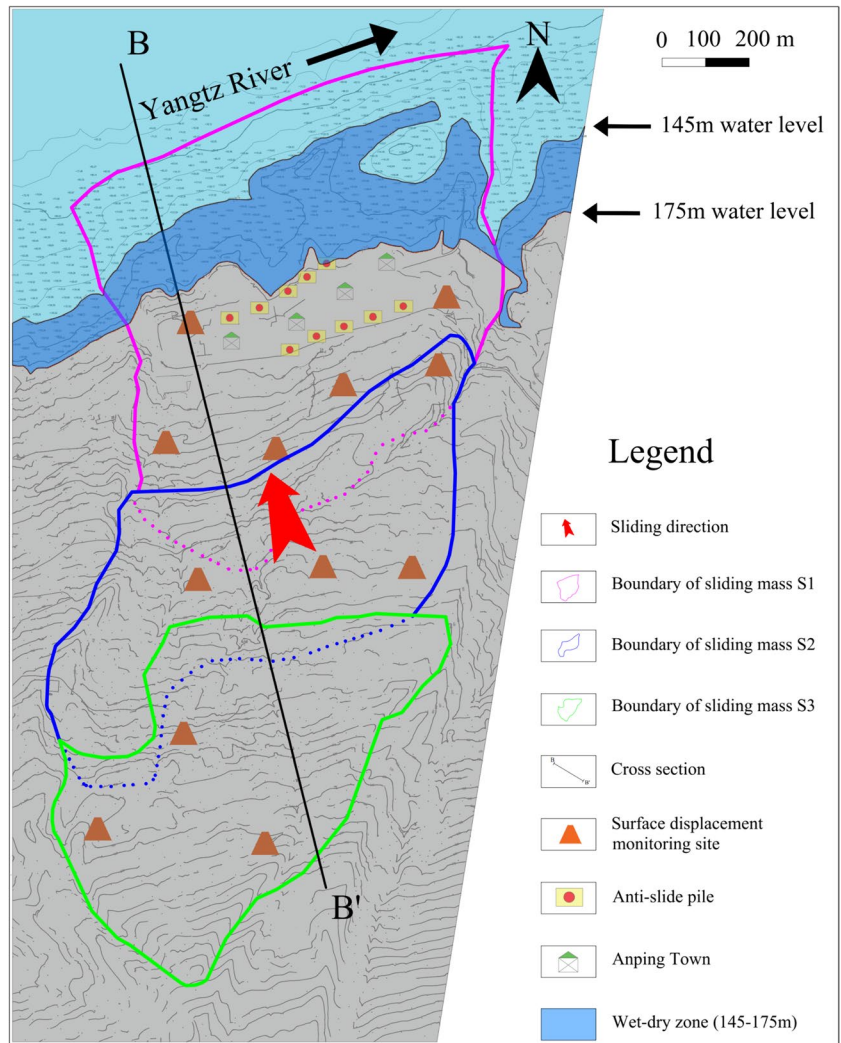

(a)

(b)

Fig. 2 Overview of the Outang landslide. **a** Location of the Outang landslide; **b** Remote image of the Outang landslide

Fig. 3 Engineering geological map of the Outang landslide

Fig. 4 Geological cross-section of Outang landslide (see B-B' profile location in Fig. 3)

sizes have been identified in the landslide area since the impoundment of the TGR in 2003 (Luo and Huang 2020). The leading edge of the sliding mass S1 is influenced by the fluctuation of the reservoir water level, causing the collapse and damage of steep slope soil and rock within the wet-dry zone along the riverfront, resulting in severe degradation of the soil and rock. The sliding mass S2 is not affected by the reservoir water level. Field investigations reveal fewer and smaller surface deformations in this area, furthermore, these deformations are primarily induced by heavy rainfall and exhibit negligible progression during the dry season. The sliding mass S3 is predominantly influenced by precipitation. In response to intense rainfall, the fractured rock mass at the leading edge of this area undergoes deformation towards the unconstrained space, resulting in the development of fissure grooves on the rear slope and surface cracking in residential buildings (Fig. 5).

The investigation and analysis of the macroscopic deformation of the Outang landslide indicate that the primary factors contributing to landslide deformation and failure are the periodic fluctuation of reservoir water level and the concentrated temporal distribution of rainfall. The lower region of the landslide is primarily influenced by the fluctuation of the reservoir water level, while the upper region is predominantly affected by rainfall. The fluctuation of reservoir water level induces the degradation of rock mass near the wet-dry zone, causing a loosening of the structure. Moreover, the rapid decline in reservoir water level generates a distinct hydraulic gradient between the interior and exterior of the slope, resulting in a pore pressure directed outward and promoting deformation in the lower region of the landslide. Concentrated rainfall enhances the weight and sliding force of the landslide mass while simultaneously weakening the mechanical strength within the sliding zone. Additionally, it erodes the superficial layer of the soil and rock mass, thereby inducing deformation in the upper region of the landslide. Consequently, it can be deduced that the failure mode of the Outang landslide corresponds to a composite push-retrogression-type landslide, which is consistent with the conclusions of Luo (Luo and Huang 2020) and Huang (Huang et al. 2020a).
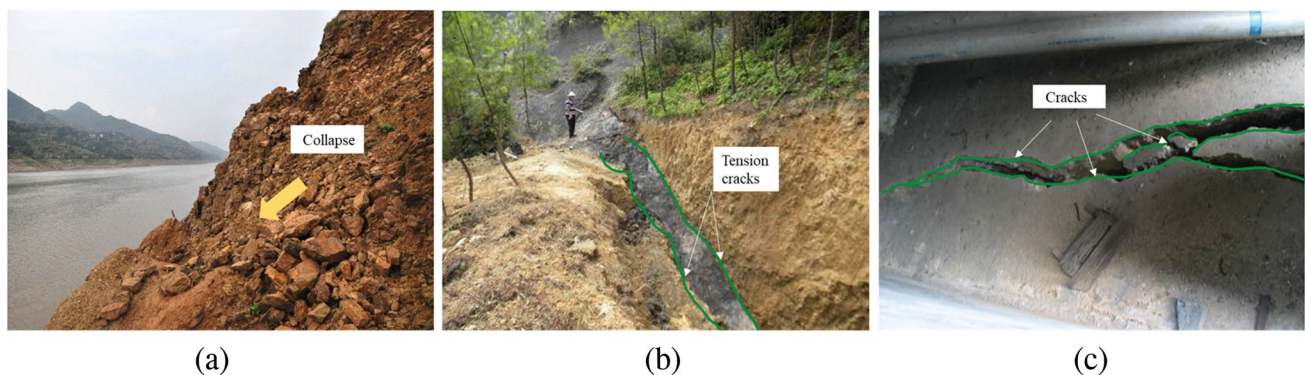
Methodology

Morgenstern-price method

The limit equilibrium method (LEM) is a typical approach for analyzing slope stability and has been widely applied in both academic and engineering fields. A variety of different LEM have been developed through continuous advancements, including the simplified Bishop method (Bishop 1955), Janbu method (Janbu 1973), Morgenstern-price method (Morgenstern and Price 1965), and Spencer method (Spencer 1967). Among these, the Morgenstern-price method incorporates all equilibrium and boundary conditions, eliminating computational errors and providing more precise solutions compared to the approximate solutions derived by Janbu. Consequently, the stability coefficient values calculated using the Morgenstern-price method exhibit a higher degree of reliability. Therefore, in this study, the Morgenstern-price method is chosen for conducting reliability analysis.

The factor of safety (*FoS*) for the corresponding sliding surface can be determined through iterative computations using this method (Factor of safety calculation formula schematic diagram is shown in Fig. 6).
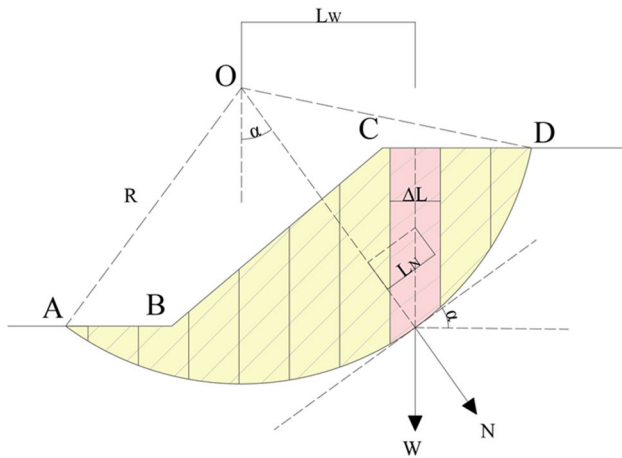
$$FoS = \frac{\sum (c\Delta LR + RN \tan \varphi)}{\sum WL_W - \sum NL_N} \tag{1}$$

$$FoS = \frac{\sum (c\Delta LR \cos \alpha + RN \tan \varphi \cos \alpha)}{\sum N \sin \alpha} \tag{2}$$

(a)   (b)   (c)

Fig. 5 Signs of landslide activity. **a** Collapse of the leading edge of the landslide (location is shown at point A in Fig. 4); **b** Tension cracks of the trailing edge of the landslide (location is shown at point B in Fig. 4); **c** Surface cracks in residential buildings (location is shown at point C in Fig. 4)

Fig. 6 Factor of safety calculation formula schematic diagram (after (Srbulov 1987))

$$N = \frac{W + \lambda f(x)\left(\frac{c\Delta L \sin \alpha}{FoS}\right) - \frac{c\Delta L \sin \alpha}{FoS}}{\left(\cos \alpha + \frac{\sin \alpha \tan \varphi}{FoS}\right) - \lambda f(x)\left(\frac{\cos \alpha \tan \varphi}{FoS} - \sin \alpha\right)}$$ (3)

Where c is the cohesive strength of the soil; φ is the frictional angle of the soil; ΔL represents the length of each soil strip on the sliding surface; L_W signifies the lever arm length from the centroid of each soil strip to the center of the sliding surface; L_N denotes the distance between the midpoint of each soil strip on the sliding surface and the corresponding normal line; α is the angle between the tangent line of each soil strip and the horizontal plane; R is the lever arm length taken with respect to the center; N represents the normal force exerted by the sliding surface on the soil strip; λ denotes the coefficient of variation of the interstrip force; $f(x)$ signifies the function describing the variation of the interstrip force.

Unsaturated shear strength theory

The shear strength of unsaturated soil differs from that of saturated soil due to the influence of matric suction. Considering that the saturation state of reservoir bank slopes constantly changes under reservoir water fluctuations, accurate determination of the shear strength of unsaturated soil holds paramount importance for slope stability analysis. The shear strength expression for unsaturated soil can be expressed as follows (Fredlund et al. 1978):

$$\tau f = c' + (\sigma - ua) \tan \varphi' + (ua - uw) \tan \varphi^b$$ (4)

Where τ_f represents the shear strength of the failure surface; c' denotes the effective cohesion; φ' denotes the effective frictional angle; σ is the total stress on the failure

surface; u_a signifies the pore air pressure; u_w signifies the pore water pressure; $(u_a - u_w)$ represents the matric suction; φ^b denotes the rate at which the shear strength varies with an increase in matric suction.

Random field theory

In traditional geotechnical engineering uncertainty analysis, soil and rock parameters are frequently regarded as random variables in order to investigate the influence of parameter uncertainty on engineering reliability. However, the random field theory proposed by Vanmarcke in 1977 is an extension of random theory in spatial terms (Vanmarcke 1977), which can better reflect the spatial correlation of soil and rock parameters. As shown in Fig. 7a (Phoon and Kulhawy 1999), a random field can be regarded as consisting of two components: trend component and fluctuation component (deviation from trend line):

$$\zeta(z) = t(z) + \omega(z)$$ (5)

Where z represents the spatial position. The trend component, denoted as $t(z)$, is associated with z. When the trend component $t(z)$ is constant, specifically equal to the mean μ, the fluctuation component $\omega(z)$ does not exhibit changes in its standard deviation and mean across different spatial positions z. Furthermore, if the correlation of the fluctuation component $\omega(z)$ is solely determined by the fluctuation range of the random field, it is referred to as a stationary random field.

Within the spatial domain, there exists autocorrelation among soil and rock parameters, which needs to be described using autocorrelation functions. The mean and variance of the random field of parameter ζ can be defined as follows:

$$E(\zeta(z)) = \mu$$ (6)

$$Var(\zeta(z)) = \sigma^2$$ (7)

Where μ represents the mean and σ^2 represents the variance.

The covariance function between any two points, denoted as $\zeta(z_i)$ and $\zeta(z_j)$, of the soil and rock parameters within the spatial domain can be expressed as follows:

$$Cov[\zeta(z_i), \zeta(z_j)] = E[(X(z_i) - \mu(z_i)) \cdot (X(z_j) - \mu(z_j))]$$ (8)

In practical engineering applications, it is common to employ theoretical autocorrelation functions for computational analysis, which serve as approximations to the actual autocorrelation functions. Among these, the Markovian theoretical autocorrelation function expressed as follows:
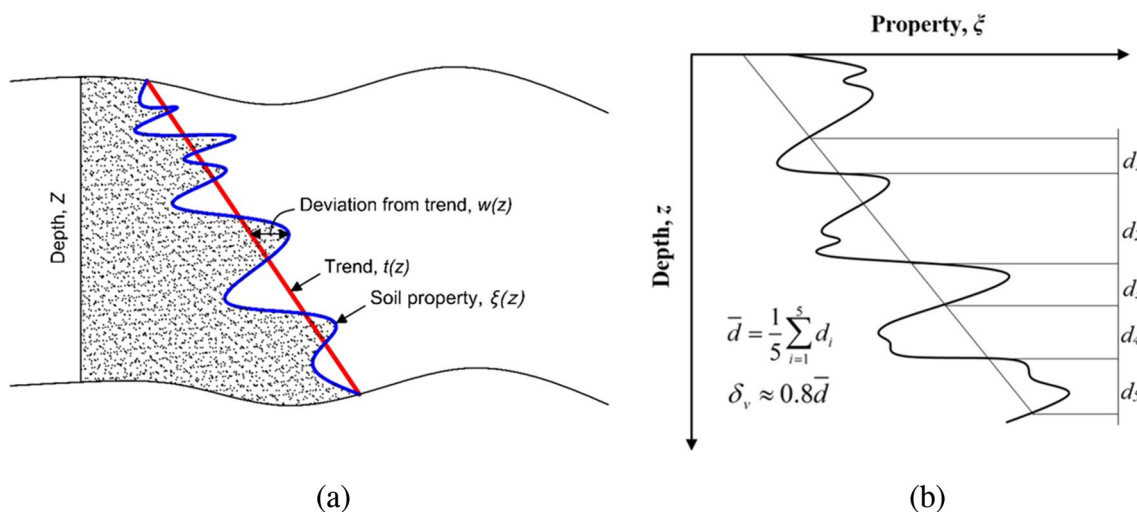
Fig. 7 **a** Conceptual diagram of random field theory (after Phoon and Kulhawy 1999); **b** A typical representation of the vertical scale of fluctuation (after Chakraborty and Dey 2022)

$$\rho\left(\tau_x, \tau_y\right) = \exp\left[-\sqrt{\left(\frac{2\tau_x}{\delta_h}\right)^2 + \left(\frac{2\tau_y}{\delta_v}\right)^2}\right] \tag{9}$$

Where τ_x and τ_y represent the horizontal relative distance and vertical relative distance, respectively; δ_h and δ_v represent the horizontal and vertical fluctuation ranges, respectively (A typical representation of the vertical scale of fluctuation is shown in Fig. 7b (Chakraborty and Dey 2022)).

Monte Carlo simulation

Monte Carlo method is a statistical sampling-based approach for studying random variables. The methodology involves generating random variable samples that conform to a certain distribution through sampling. Subsequently, corresponding functional samples are obtained based on structural functional functions. Finally, the failure probability is determined by calculating the proportion of failure samples through statistical analysis. In the analysis of slope stability, failure samples can be defined as follows:

$$F = \left\{F_s(x) < f_s\right\} \tag{10}$$

Where x represents random variable; f_s represents the threshold value of the safety factor, the probability of slope failure can be defined as follows:

$$P_f = \int_F f(x)d_x \tag{11}$$

Where $f(x)$ is the probability density function of the random variable x.

According to the theory of Monte Carlo simulation, random sample $x_i(i = 1, 2, 3 \cdots, N)$ is first generated through sampling based on $f(x)$, and then $F_s(x_i)$ is calculated according to the slope safety solution method. The failure probability of the slope can be expressed as follows:

$$P_f = \frac{1}{N} \sum_{i=1}^{N} M_i \tag{12}$$

Where M denotes the indicator function; If $F_s(x_i) < f_s$, then $M_i = 1$, otherwise $M_i = 0$.

Parameter selection and working condition setting

Numerical calculation model of the Outang landslide

Based on the engineering characteristics and geological features of the Outang landslide, the B-B′ section was selected for calculating the factor of safety (*FoS*) and failure probability (P_f). A two-dimensional saturated–unsaturated seepage slope stability model was established in SLIDE2 (Fig. 8). Taking into account the overall stability of the Outang landslide was controlled by the weak interlayer, the weak interlayer is designated as the sliding zone. To facilitate modeling convenience and enhance computational efficiency, sliding zone I, II and III are connected as a whole sliding zone through the body of the slope, as shown in Fig. 8. In order to reveal the relative role of different areas in the landslide, the model is divided into six parts: part 1 is the upper layer composed of silty clay with crushed stone; part 2 is the lower
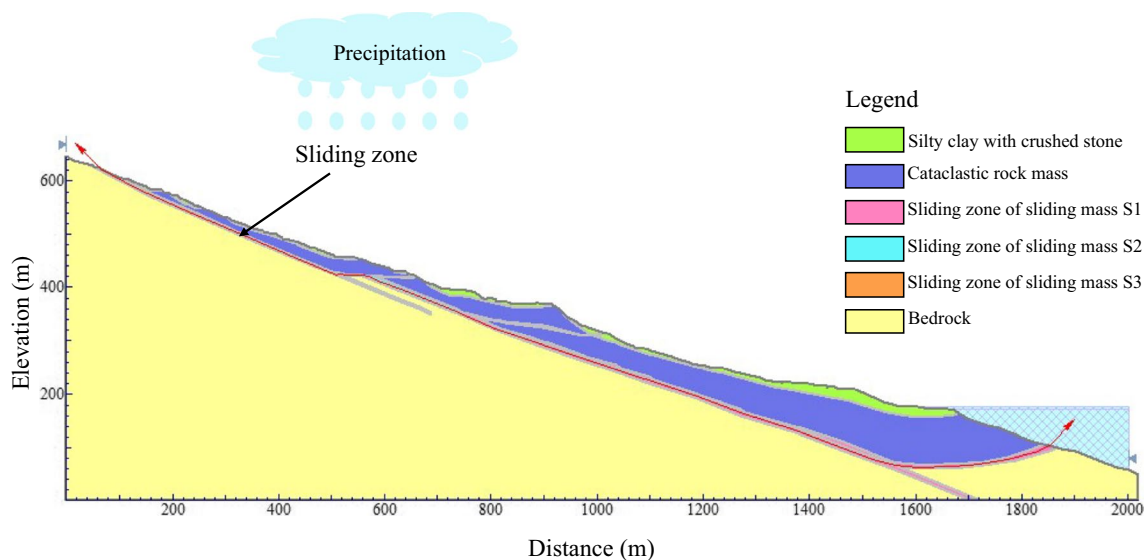
Fig. 8 Numerical model of the Outang landslide

layer composed of cataclastic rock mass; part 3 is the sliding zone I; part 4 is the sliding zone II; part 5 is the sliding zone III and part 6 is the bedrock.

According to the meteorological, hydrological, and geological conditions in the Outang landslide area, the boundaries of the computational model were established as follows: the leading edge below 145 m is consistently submerged by reservoir water throughout the year, and thus it is designated as a fixed water head boundary. The slope surface with an elevation ranging from 145 to 175 m is influenced by the fluctuation in reservoir water level, resulting in the implementation of a variable water head boundary. The area above 175 m is primarily affected by rainfall, and the boundary condition is determined by the intensity of precipitation. Survey data indicates minimal annual variations in the water level at the rear of the landslide mass, leading to the assignment of a fixed water head boundary at an elevation of 588 m for the trailing edge, while the bottom boundary is defined as impervious boundary.

Selection of geotechnical parameters

The Mohr–Coulomb model is selected to characterize the mechanical properties of the landslide. The hydraulic and mechanical parameters of the Outang landslide used in this study are adopted from the relevant literature and engineering geologic analogy (Luo and Huang 2020; Luo et al. 2020; Zhang et al. 2023; Zhou et al. 2023). In order to evaluate the relative significance of different regions in relation to landslide stability, the influence of variations in the statistical mechanical parameters of different regions on the failure probability is considered. Specifically, parameters

c and φ of the Outang landslide are assumed to follow lognormal distribution in this study. Furthermore, the statistical characteristics of shear strength parameters demonstrate significant variations among different soil types, therefore, accurately determining these statistical mechanical parameters is crucial for the precision of numerical simulations. The research object of this study is the Outang landslide located in the Three Gorges Reservoir area. Based on existing literature and cases, the Zhao Shuling landslide which is located in the Three Gorges Reservoir area, was selected as a reference (Zhang et al. 2023). The coefficient of variation of cohesion (COVc) for the sliding mass and sliding zone is assumed to be 0.3, while the coefficient of variation of frictional angle (COVφ) is assumed to be 0.2. The default correlation coefficient ($\rho_{c,\varphi}$) is assumed to be -0.5. Additionally, the horizontal scale of fluctuation (δ_h) for the sliding mass is set to 40 m, with the vertical scale of fluctuation (δ_v) is considered to be 4 m, whereas for the sliding zone, the δ_h is set to 20 m, with the δ_v is considered to be 2 m.

The physical and mechanical parameters of the landslide are listed in Table 1, and the statistical mechanical parameters of the landslide are listed in Table 2.

Design of working conditions

According to the survey data, it is evident that the regulation pattern of the reservoir water level in the TGR area remains consistent throughout the year, approximately comprising five distinct stages. Stage I (January 1st—March 20th): the water level gradually decreases from 175 to 165 m, indicating a slow descending stage; stage II (March 21st—June

Table 1 Physical and mechanical parameters of the landslide

Soil type	Unit weight γ (kN/m^3)	Cohesion c (kPa)	Friction angel φ (°)	WC sat θ_s (m^3/m^3)	WC res θ_r (m^3/m^3)	Permeability coefficient K_s (m/s)
Silty clay with crushed stone	20.5	16	14.6	0.32	0.09	1.22×10^{-5}
Cataclastic rock mass	26	70	16.2	0.275	0.09	3.01×10^{-6}
Sliding zone I	21	8	16.5	0.3	0.05	5.79×10^{-7}
Sliding zone II	21	12	16.8	0.3	0.05	5.79×10^{-7}
Sliding zone III	21	23	16.5	0.3	0.05	5.79×10^{-7}
Bedrock	27.6	700	42	0.05	0	3.47×10^{-8}

Table 2 Statistical mechanical parameters of the landslide

Soil type	Parameters	Mean	COV	Distribution	Scale of fluctuation	Correlation coefficient
Silty clay with crushed stone	c	16	0.3	Lognormal	$\delta_h = 40$ m	-0.5
	φ	14.6	0.2		$\delta_v = 4$ m	
Cataclastic rock mass	c	70	0.3	Lognormal	$\delta_h = 40$ m	-0.5
	φ	16.2	0.2		$\delta_v = 4$ m	
Sliding zone I	c	8	0.3	Lognormal	$\delta_h = 20$ m	-0.5
	φ	11.3	0.2		$\delta_v = 2$ m	
Sliding zone II	c	12	0.3	Lognormal	$\delta_h = 20$ m	-0.5
	φ	16	0.2		$\delta_v = 2$ m	
Sliding zone III	c	23	0.3	Lognormal	$\delta_h = 20$ m	-0.5
	φ	15.5	0.2		$\delta_v = 2$ m	
Bedrock	c	700	-	-	-	-
	φ	42	-			

10th): the water level rapidly drops from 165 to 145 m, representing a rapid descending stage; stage III (June 11th—August 20th): the water level fluctuates between 145 and 155 m; stage IV (August 21st—October 20th): the water level ascends from 145 to 175 m, corresponding to a rising stage; stage V (October 21st—December 31st): the water level mainly stabilizes at 175 m without significant variations.

Utilizing the actual daily variation data of reservoir water level and precipitation in 2014 as the transient boundary conditions of the slope (Fig. 13 illustrates the variations in reservoir water level and daily rainfall in 2014), thus the stability variation of the landslide within a one-year cycle can be computed.

Results and discussion

Sensitivity analysis

To explore the impact of diverse statistical mechanical parameters on slope stability, we specifically selected rainfall and reservoir water level data from a single day. As a demonstration, sensitivity analysis was performed through failure probability calculations. For the purpose of this investigation, data from June 10th were utilized for analysis, this analysis focuses on the coefficient of variation, correlation coefficient, fluctuation range of cohesion (c) and frictional angle (φ), as well as the autocorrelation function. The primary objective is to investigate the impact of varying values of the random field correlation parameters on the failure probability. Moreover, in order to ascertain the relative significance of different regions in influencing slope stability, the effects of variations in statistical mechanical parameters within distinct regions on the failure probability are taken into consideration. Specifically, this study analyzes the following five regions: whole sliding zone, sliding zone I, sliding zone II, sliding zone III and sliding zone with sliding mass.

In the probabilistic analysis, the variation of statistical mechanical parameters of different regions in the landslide is taken into account respectively. Subsequently, the calculated failure probability (P_f) for different regions is compared with the overall (sliding zone with sliding mass) failure probability, therefore, it can be deduced that a smaller disparity between an individual region and the entirety signifies a greater significance of that region in controlling the slope stability.

The effect of the COV

The coefficient of variation for both cohesion (c) and frictional angle (φ) ranges from 0.1 to 0.5. When evaluating the impact of varying one parameter, keep the coefficient of variation of the other parameter constant. The random field parameters are selected according to Table 2. When considering the overall coefficient of variation (COV) changes for the sliding mass and sliding zone, as illustrated in Fig. 9, it can be observed that as COVφ varies from 0.1 to 0.5, the failure probability increases from 2.87% to 32.22%. Similarly, when COVc varies from 0.1 to 0.5, the failure probability increases from 7.95% to 8.62%. In general, both cohesion and frictional angle contribute to an increase in the failure probability of the slope as the COV increases, indicating that a higher degree of variability in the strength parameters adversely affects slope stability. By comparing the trend of the curves in Fig. 9a and b, it becomes evident that the variability in the frictional angle (φ) has a greater influence on the failure probability.

In addition, the results of the probabilistic analysis reveal the relative importance of different regions on the stability of the Outang landslide (as shown in Fig. 9). Firstly, the stability of the Outang landslide is primarily influenced by the sliding zone, while the sliding mass has a minimal impact on the stability of the landslide. Secondly, among the three sliding zones, sliding zone I exerts the greatest influence on the slope stability, followed by sliding zone III.
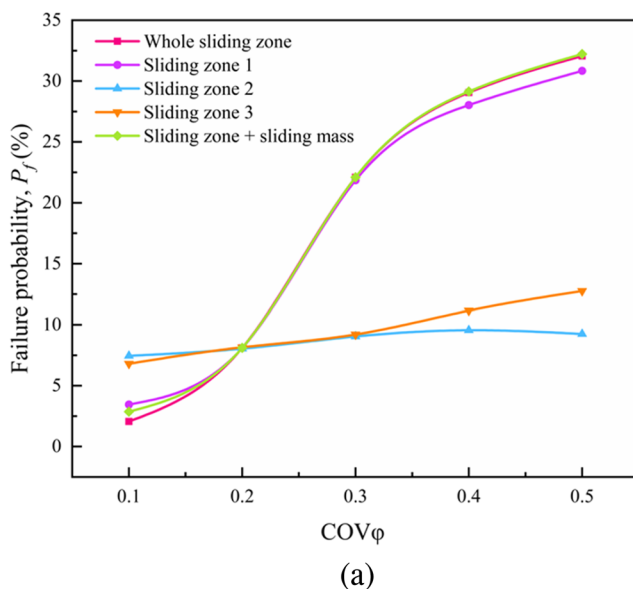
The effect of the correlation coefficient

The correlation between cohesion (c) and frictional angle (φ) in the soil and rock mass is represented by the correlation coefficient $\rho_{c,\varphi}$. Considering the impact of the correlation coefficient $\rho_{c,\varphi}$ between c and φ on the failure probability, the correlation coefficient $\rho_{c,\varphi}$ is selected to be -0.7, -0.5, -0.3, -0.1, 0.1, and 0.3, respectively. The remaining statistical parameters of the random field are determined based on Table 2. The result obtained under different correlation coefficients is illustrated in Fig. 10. When considering the overall correlation coefficient changes for the sliding mass and sliding zone, as illustrated in Fig. 10, it can be observed that as the correlation coefficient varies from -0.7 to 0.3, the failure probability increases from 7.75% to 8.92%. This indicates that a higher magnitude of the correlation coefficient corresponds to an increase in the failure probability, implying that a stronger negative correlation is associated with a lower failure probability. However, in terms of the actual values of the failure probability, there is not a significant change with variations in the correlation coefficient. Furthermore, Fig. 10 also reveals the relative importance of different regions on the stability of the Outang landslide, which is consistent with the conclusions drawn earlier.

The effect of the autocorrelation function and the fluctuation

SLIDE2 incorporates three built-in autocorrelation functions: Markovian 1D Separable, Markovian, and Gaussian. This study aims to investigate the influence of these three
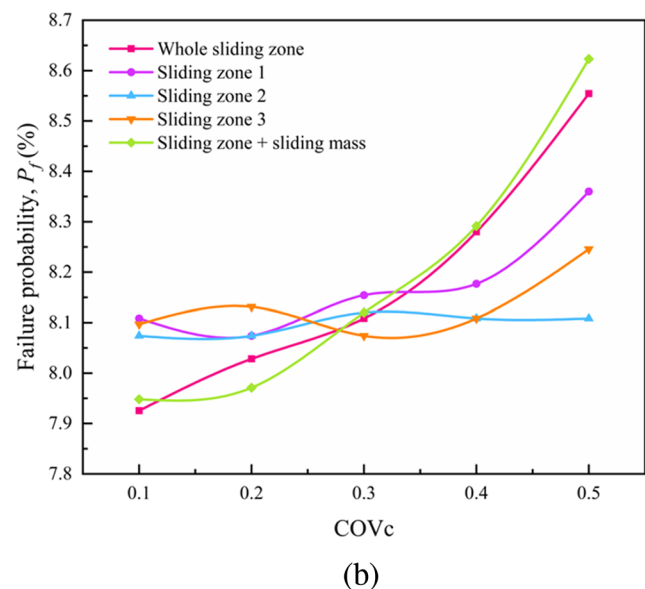

Fig. 9 Influence of COV on failure probability. **a** COVφ; **b** COVc
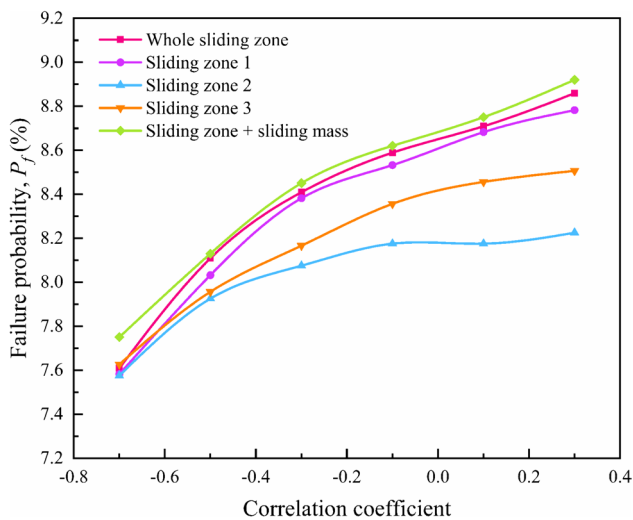
Fig. 10 Influence of correlation coefficient on failure probability

autocorrelation functions on the reliability of the Outang landslide. Additionally, the effects of variability in shear strength parameters and different ranges of fluctuations are considered. Specifically, the ranges for COVc and COVφ are set between 0.1 and 0.5, while the horizontal and vertical ranges of fluctuation for shear strength parameters (δ_h and δ_v, respectively) are chosen as 10 m to 80 m and 1 m to 8 m, respectively. During the parameter sensitivity analysis, it is assumed that when one parameter undergoes changes, the remaining parameters remain constant. From Fig. 11, it can be observed that the failure probability of the Outang landslide increases as the COV for the strength parameters increases. Additionally, the failure probability

of the landslide is also affected by different autocorrelation functions to some extent. Particularly, when the COV for the strength parameters is relatively small, the impact of various autocorrelation functions on the failure probability of the landslide becomes more prominent.

When considering the autocorrelation function as Markovian, an analysis of Fig. 12 reveals that the failure probability increases from 7.35% to 12.40% as δ_h varies from 10 to 80. Similarly, when δ_v varies from 1 to 8, the failure probability rises from 6.33% to 14.30%. These data indicate that an increase in the scale of horizontal or vertical fluctuations corresponds to a gradual increment in the failure probability, implying a decrease in slope stability. Comparing the trend of the curves in Fig. 12a and b, it can be inferred that the variation of the failure probability is more significantly influenced by the vertical scale of fluctuation (δ_v). Furthermore, Fig. 12 highlights that when the horizontal scale of fluctuation is small, the influence of different autocorrelation functions on the failure probability becomes relatively apparent. Conversely, when the vertical scale of fluctuation is large, the influence of different autocorrelation functions on the failure probability becomes more prominent. In summary, the impact of different autocorrelation functions on the failure probability of the Outang landslide is more pronounced when the soil strength parameter coefficient of variation is small and the vertical scale of fluctuation is large.

Calculation of annual stability

The calculation of overall stability of the Outang landslide in a complete annual cycle was computed in SLIDE2, with a selected time step of one day. The computed factor of safety
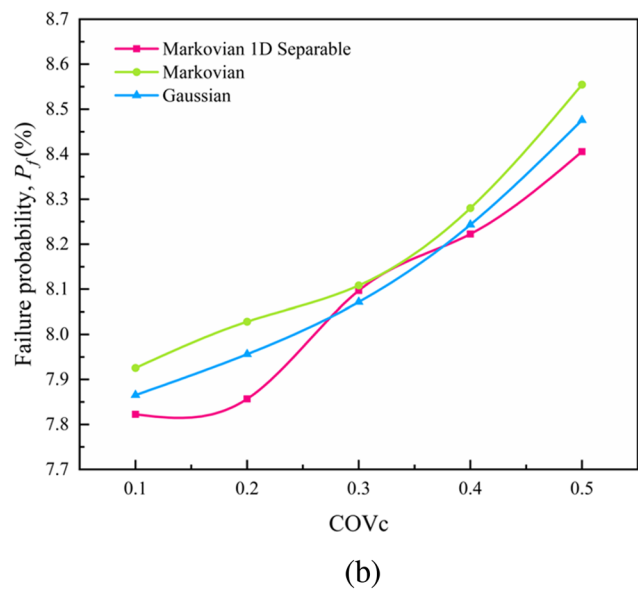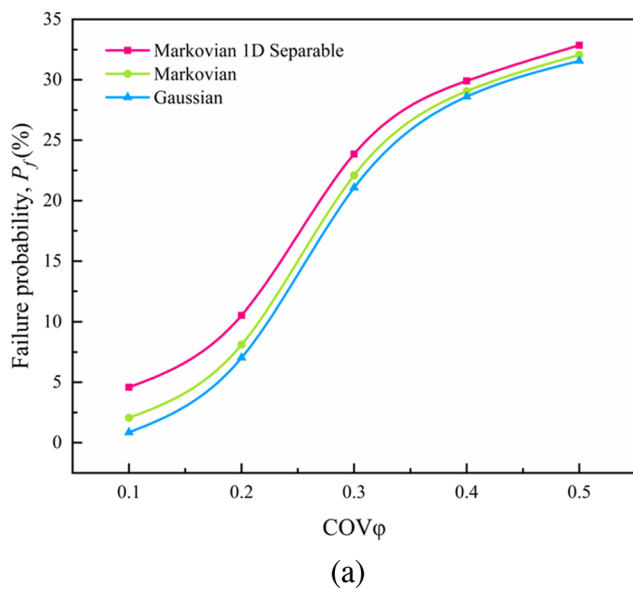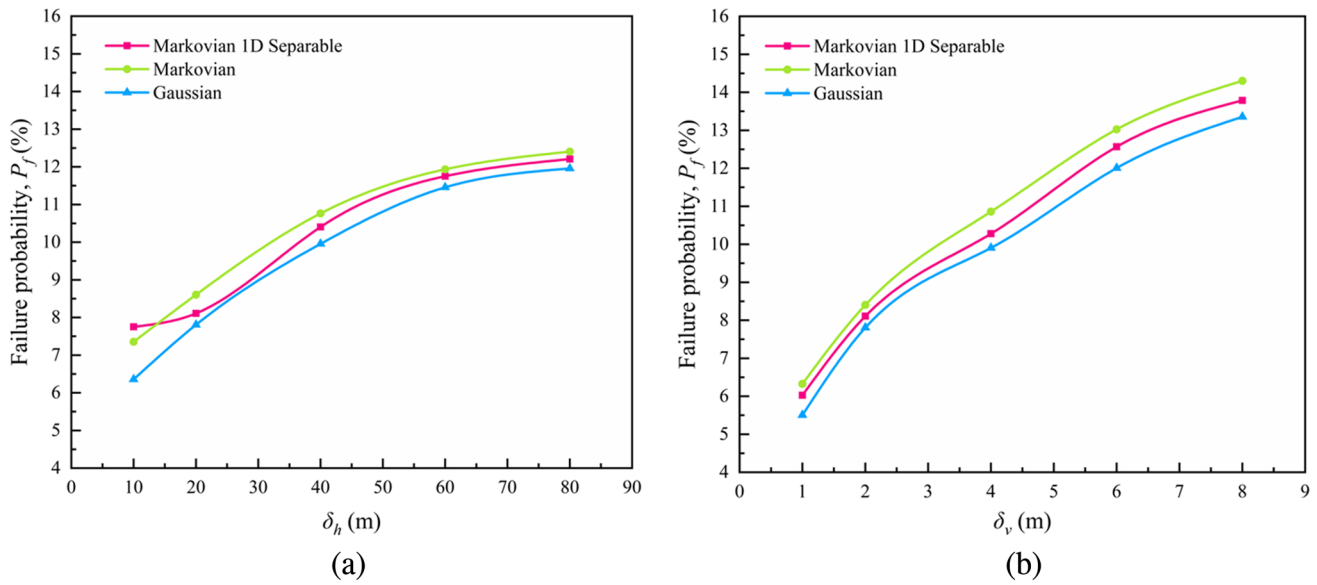

Fig. 11 Influence of autocorrelation function and COV on failure probability. **a** COVφ; **b** COVc

Fig. 12 Influence of autocorrelation function and scale of fluctuation on failure probability. **a** Horizontal scale of fluctuation (δ_h); **b** Vertical scale of fluctuation (δ_v)

(*FoS*) changes within a one-year cycle is illustrated in Fig. 13. The *FoS* varies between 1.18 and 1.27 throughout the year. Notably, the *FoS* decreases during the period of water level drawdown and increases in the impoundment period. This observation implies a close relationship between slope stability and the fluctuation of the reservoir water level. Specifically, the declination of water level is detrimental to the stability of the slope, while the increase of water level is conducive. The substantial decline in reservoir water level started on May 2nd, while the noticeable decrease in the *FoS* began on May 5th, suggesting that the fluctuation in reservoir water level has a lagging effect on slope stability. In general, there is a strong consistency and synchronicity between the changes in the *FoS*

and the reservoir water level. This indicates that the fluctuation in the reservoir water level serves as the predominant controlling factor influencing the stability of the Outang landslide, whereas the impact of rainfall is comparatively limited. Nevertheless, due to the effect of rainfall, the variation curve of *FoS* is not as smooth as the fluctuation schedule.

Calculation of annual reliability

Stage I (January 1st ~ March 20th)

During this stage, the reservoir water level gradually decreases and rainfall is minimal. As shown in Fig. 14a,

Fig. 13 Annual variation of rainfall, reservoir water level and factor of safety
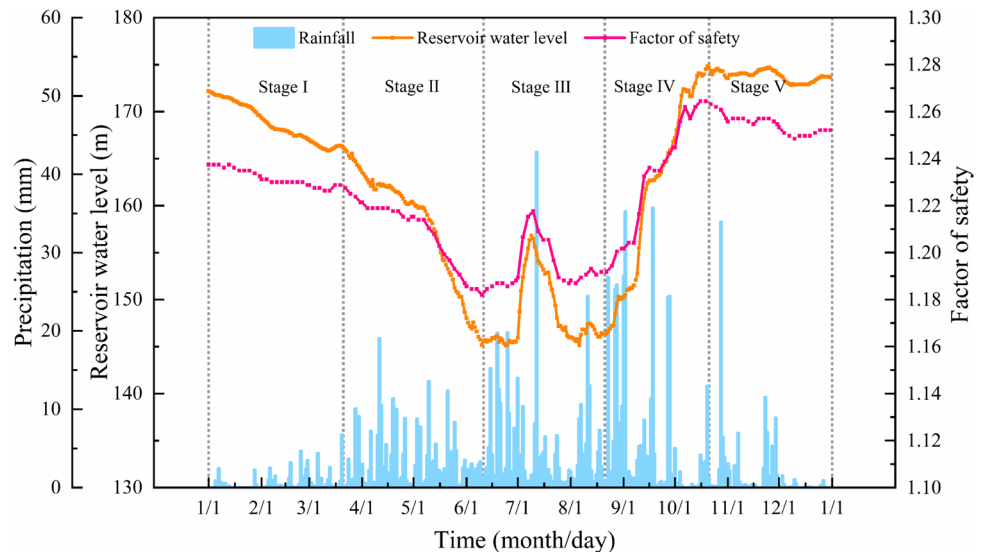
the highest failure probability of the slope is 4.64%, while the lowest is 2.77%. Although there are fluctuations, they remain at a relatively low level, indicating that external factors have a minimal impact on slope stability during this stage. The variation curve of the failure probability during this stage reveals more subtle phenomena compared to the safety factor variation curve, for instance, between February 3rd and February 20th, the variation curve of the safety factor shows minimal changes, resembling a straight line, whereas the failure probability curve demonstrates a

process of initial decrease followed by an increase. This observation indicates a higher sensitivity of failure probability to changes in rainfall and reservoir water level.

Stage II (March 21st ~ June 10th)

During this stage, the decrease rate of reservoir water level significantly accelerated, accompanied by a gradual increase in rainfall intensity and frequency. As shown in Fig. 14b, the slope failure probability rises from 4.43% to 8.10%.
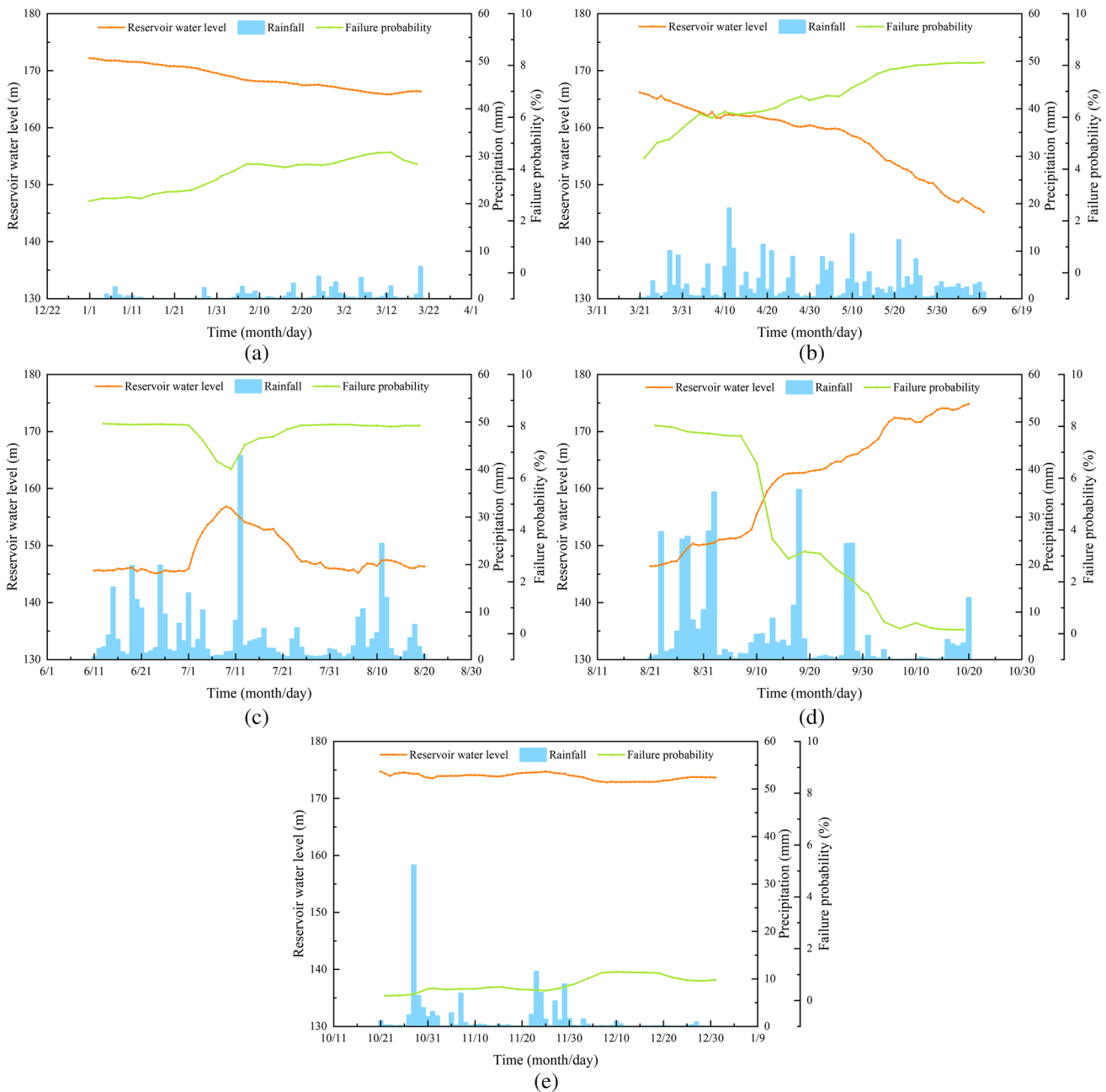
Fig. 14 Variation of failure probability of different stages. **a** Stage I; **b** Stage II; **c** Stage III; **d** Stage IV; **e** Stage V

This observation indicates that as the reservoir water level decreases, the slope stability gradually diminishes as well. Moreover, a faster decline in reservoir water level results in a higher failure probability, aligning with the findings of conventional deterministic analysis. In general, the failure probability of the slope is primarily influenced by changes in the reservoir water level, with rainfall being a secondary factor.

Stage III (June 11th ~ August 20th)

During this stage, the variation curve of the failure probability remains closely correlated with changes in reservoir water level, but there are differences observed in certain periods, as shown in Fig. 14c. From July 1st to July 10th, as the reservoir water level rises, the failure probability rapidly decreases to 6.35%. Subsequently, as the reservoir water level declines until July 25th, the failure probability exhibits a rapid increase. These findings suggest that an increase in reservoir water level favors slope stability, which is consistent with conventional deterministic analysis. However, during the period from August 5th to August 15th, despite a rise in reservoir water level, it does not lead to a decrease in failure probability, possibly due to the influence of rainfall, maintaining the failure probability at a relatively high level.

Stage IV (August 21st ~ October 20th)

During this stage, the reservoir water level continues to rise, while rainfall remains at a relatively high level. As shown in Fig. 14d, the slope failure probability decreases from 8.02% to 0.15%. It is noteworthy that between October 4th and October 20th, the failure probability exhibits slight fluctuations at a low level, while the safety factor continues to increase (Fig. 13). This can be attributed to the fact that the failure probability is already very small during this period, leaving limited room for further decline. Therefore, in situations where the failure probability is already small, it fails to effectively reflect the changes in slope stability.

Stage V (October 21st ~ December 31st)

During this stage, the reservoir water level remains essentially constant at a high level of 175 m, and the rainfall significantly decreases compared to previous periods, as shown in Fig. 14e. The failure probability curve during this stage exhibits a trend of initial stability, followed by an increase, and then stable fluctuations. The decline in slope stability during this period may be attributed to the prolonged influence of the high reservoir water level, which leads to the degradation of the physical and mechanical properties of the slope's rock and soil mass.

Through the analysis of the annual stability and annual reliability of the Outang landslide, it is evident that the results obtained from deterministic analysis and probabilistic analysis are generally consistent. However, probabilistic analysis exhibits greater sensitivity to changes in rainfall and reservoir water level, allowing for the observation of more subtle variations. Nonetheless, probabilistic analysis also presents certain limitations, such as its inability to effectively reflect changes in slope stability in situations where the slope safety factor is already high and the failure probability is small. To fully leverage the advantages of both deterministic analysis and probabilistic analysis, it is recommended to conduct stability evaluations of slopes in practical engineering projects through the combined use of deterministic analysis and probabilistic analysis.

Conclusions

Based on the monitored data of the hydrologic conditions from 2014, the Outang landslide in the TGR is studied under the combined effect of rainfall and reservoir water level fluctuation. Sensitivity analyses of the coefficient of variation, correlation coefficient, the scale of fluctuation and autocorrelation functions were conducted using the numerical model established by SLIDE2, subsequently, the annual variation of factor of safety and failure probability of five representative stages were calculated. Several conclusions can be drawn as follows:

(1) The results of the probabilistic analysis reveal the relative importance of different regions on the stability of the Outang landslide. The overall stability of the landslide is primarily governed by the sliding zone, with sliding zone I demonstrating the most pronounced influence on slope stability, followed by sliding zone III.

(2) The spatial variability of soil strength parameters had a significant impact on the failure probability of the slope. The failure probability demonstrates an increasing trend with the elevation of the COV, correlation coefficient, and the scale of fluctuation, respectively, and the COV has the greatest impact on the failure probability, followed by the scale of fluctuation, and finally the correlation coefficient. Nevertheless, the variation of the failure probability is more significantly influenced by the frictional angle (φ) and vertical scale of fluctuation (δ_v). Furthermore, the impact of different autocorrelation functions on the failure probability of the Outang landslide is more pronounced when the soil strength parameter coefficient of variation is small and the vertical scale of fluctuation is large.

(3) The stability of the Outang landslide decreases during the period of water level drawdown and increases in the impoundment period, and fluctuation in reservoir water level has a lagging effect on the slope stability. Meanwhile, the variation curve of the failure probability reveals more subtle phenomena compared to the safety factor variation curve, in order to fully leverage the advantages of deterministic analysis and probabilistic analysis, it is recommended to employ a combined approach of deterministic analysis and probabilistic analysis for slope stability assessment in practical engineering. In general, the stability of the Outang landslide is predominantly governed by the water level fluctuation, with the impact of rainfall being comparatively negligible.

References

Bishop AW (1955) The use of the slip circle in the stability analysis of slopes. Geotechnique 5:7–17

Chakraborty R, Dey A (2022) Probabilistic slope stability analysis: state-of-the-art review and future prospects. Innov Infrastruct So 7:177

Chen ML, Lv PF, Zhang SL, Chen XZ, Zhou JW (2018) Time evolution and spatial accumulation of progressive failure for xinhua slope in the dagangshan reservoir, southwest china. Landslides 15:565–580. https://doi.org/10.1007/s10346-018-0946-8

Chen ML, Qi SC, Lv PF, Yang XG, Zhou JW (2021) Hydraulic response and stability of a reservoir slope with landslide potential under the combined effect of rainfall and water level fluctuation. Environ Earth Sci 80. https://doi.org/10.1007/s12665-020-09279-7

Ching JY, Hu YG, Yang ZY, Shiau JQ, Chen JC, Li YS (2011) Reliability-based design for allowable bearing capacity of footings on rock masses by considering angle of distortion. Int J Rock Mech Min Sci 48:728–740. https://doi.org/10.1016/j.ijrmms.2011.05.005

Deng ML, Huang XH, Yi QL, Liu YL, Yi W, Huang HF (2023) Fifteen-year professional monitoring and deformation mechanism analysis of a large ancient landslide in the three gorges reservoir area, china. Bull Eng Geol Environ 82:243

Fredlund DG, Morgenstern NR, Widger RA (1978) Shear-strength of unsaturated soils. Can Geotech J 15:313–321. https://doi.org/10.1139/t78-029

Griffiths DV, Fenton GA (2004) Probabilistic slope stability analysis by finite elements. J Geotech Geoenviron Eng 130:507–518. https://doi.org/10.1061/(asce)1090-0241(2004)130:5(507)

Gu X, Chen FY, Zhang WA, Wang Q, Liu HL (2022) Numerical investigation of pile responses induced by adjacent tunnel excavation in spatially variable clays. Underg Space 7:911–927. https://doi.org/10.1016/j.undsp.2021.09.003

He XG, Hong Y, Vergara H, Zhang K, Kirstetter PE, Gourley JJ, Zhang Y, Qiao G, Liu C (2016) Development of a coupled hydrological-geotechnical framework for rainfall-induced landslides prediction. J Hydrol 543:395–405. https://doi.org/10.1016/j.jhydrol.2016.10.016

Huang FM, Huang JS, Jiang SH, Zhou CB (2017) Landslide displacement prediction based on multivariate chaotic model and extreme learning machine. Eng Geol 218:173–186. https://doi.org/10.1016/j.enggeo.2017.01.016

Huang D, Luo SL, Zhong Z, Gu DM, Song YX, Tomas R (2020a) Analysis and modeling of the combined effects of hydrological factors on a reservoir bank slope in the three gorges reservoir area, china. Eng Geol 279. https://doi.org/10.1016/j.enggeo.2020.105858

Huang XH, Guo F, Deng ML, Yi W, Huang HF (2020b) Understanding the deformation mechanism and threshold reservoir level of the floating weight-reducing landslide in the three gorges reservoir area, china. Landslides 17:2879–2894. https://doi.org/10.1007/s10346-020-01435-1

Janbu N (1973) Slope stability computations. Publication of, Wiley Sons, Incorporated

Jian WX, Xu Q, Yang HF, Wang FW (2014) Mechanism and failure process of qianjiangping landslide in the three gorges reservoir, china. Environ Earth Sci 72:2999–3013. https://doi.org/10.1007/s12665-014-3205-x

Jiang JW, Ehret D, Xiang W, Rohn J, Huang L, Yan SJ, Bi RN (2011) Numerical simulation of qiaotou landslide deformation caused by drawdown of the three gorges reservoir, china. Environ Earth Sci 62:411–419. https://doi.org/10.1007/s12665-010-0536-0

Jiang SH, Huang JS, Griffiths DV, Deng ZP (2022) Advances in reliability and risk analyses of slopes in spatially variable soils: a state-of-the-art review. Comput Geotech 141. https://doi.org/10.1016/j.compgeo.2021.104498

Jiao YY, Zhang HQ, Tang HM, Zhang XL, Adoko AC, Tian HN (2014) Simulating the process of reservoir-impoundment-induced landslide using the extended dda method. Eng Geol 182:37–48. https://doi.org/10.1016/j.enggeo.2014.08.016

Li DY, Yin KL, Leo C (2010) Analysis of baishuihe landslide influenced by the effects of reservoir water and rainfall. Environ Earth Sci 60:677–687. https://doi.org/10.1007/s12665-009-0206-2

Li Z, He YJ, Xu HF, Yang Y (2015) Model test study on landslide of reservoir bank near dam under antecedent rainfall. 4th International Conference on Sustainable Energy and Environmental Engineering (ICSEEE), Shenzhen, Peoples R. China, 180–190

Liu LL, Cheng YM, Zhang SH (2017) Conditional random field reliability analysis of a cohesion-frictional slope. Comput Geotech 82:173–186. https://doi.org/10.1016/j.compgeo.2016.10.014

Luo SL, Jin XG, Huang D, Kuang XB, Song YX, Gu DM (2020) Reactivation of a huge, deep-seated, ancient landslide: formation mechanism, deformation characteristics, and stability. Water 12. https://doi.org/10.3390/w12071960

Luo SL, Huang D (2020) Deformation characteristics and reactivation mechanisms of the outang ancient landslide in the three gorges reservoir, china. Bull Eng Geol Environ 79:3943–3958. https://doi.org/10.1007/s10064-020-01838-3

Ma JH, Yao YQ, Wei Z, Meng XM, Zhang ZL, Yin HL, Zeng RQ (2024) Stability analysis of a loess landslide considering rainfall patterns and spatial variability of soil. Comput Geotech 167:106059

McKay MD, Beckman RJ, Conover WJ (1979) A comparison of three methods for selecting values of input variables in the analysis of output from a computer code. Technometrics 21:239–245. https://doi.org/10.2307/1268522

Miao FS, Wu YP, Li LW, Liao K, Xue Y (2021) Triggering factors and threshold analysis of baishuihe landslide based on the data mining methods. Nat Hazard 105:2677–2696. https://doi.org/10.1007/s11069-020-04419-5

Morgenstern NR, Price VE (1965) The analysis of the stability of general slip surfaces. Geotechnique 15:79–93

Phoon KK, Kulhawy FH (1999) Characterization of geotechnical variability. Can Geotech J 36:612–624

Salgado R, Kim D (2014) Reliability analysis of load and resistance factor design of slopes. J Geotech Geoenviron Eng 140:57–73. https://doi.org/10.1061/(asce)gt.1943-5606.0000978

Spencer E (1967) A method of analysis of the stability of embankments assuming parallel inter-slice forces. Geotechnique 17:11–26

Srbulov MM (1987) Limit equilibrium method with local factors of safety for slope stability. Can Geotech J 24:652–656

Sun GH, Zheng H, Huang YY, Li CG (2016) Parameter inversion and deformation mechanism of sanmendong landslide in the three gorges reservoir region under the combined effect of reservoir water level fluctuation and rainfall. Eng Geol 205:133–145. https://doi.org/10.1016/j.enggeo.2015.10.014

Tu PF, Wu SC, Li HT (2011) Analysis of bazimen landslide deformation based on gps. International Conference on Energy, Environment and Sustainable Development (ICEESD 2011), Shanghai Univ Elect Power, Shanghai, Peoples R. China, 435–439

Vanmarcke EH (1977) Probabilistic modeling of soil profiles. J Geotech Eng Div-Asce 103:1227–1246

Wang LJ (2021) On the consolidation and creep behaviour of layered viscoelastic gassy sediments. Eng Geol 293. https://doi.org/10.1016/j.enggeo.2021.106298

Wang K, Zhang SJ (2021) Rainfall-induced landslides assessment in the fengjie county, three-gorge reservoir area, china. Nat Hazard 108:451–478. https://doi.org/10.1007/s11069-021-04691-z

Wang LJ, Cleall PJ, Zhu B, Chen YM (2023) Modelling the thermal-hydro-mechanical behaviour of unsaturated soils with a high degree of saturation using an extended precise integration method. Can Geotech J 60:86–101. https://doi.org/10.1139/cgj-2021-0201

Wang LQ, Wang L, Zhang WG, Meng XY, Liu SL, Zhu C (2024) Time series prediction of reservoir bank landslide failure probability considering the spatial variability of soil properties. J Rock Mech Geotech. https://doi.org/10.1016/j.jrmge.2023.11.040

Wu YP, Miao FS, Li LW, Xie YH, Chang B (2017) Time-varying reliability analysis of huangtupo riverside no.2 landslide in the three gorges reservoir based on water-soil coupling. Eng Geol 226:267–276. https://doi.org/10.1016/j.enggeo.2017.06.016

Xue Y, Wu YP, Miao FS, Li LW, Liao K, Ou GZ (2020) Effect of spatially variable saturated hydraulic conductivity with nonstationary characteristics on the stability of reservoir landslides. Stochastic Environ Res Risk Assess 34:311–329. https://doi.org/10.1007/s00477-020-01777-1

Zeng TR, Yin KL, Gui L, Peduto D, Wu LY, Guo ZZ, Li Y (2023) Quantitative risk assessment of the shilongmen reservoir landslide in the three gorges area of china. Bull Eng Geol Environ 82:214

Zhang L, Shi B, Zhang D, Sun YJ, Inyang HI (2020a) Kinematics, triggers and mechanism of majiagou landslide based on fbg real-time monitoring. Environ Earth Sci 79. https://doi.org/10.1007/s12665-020-08940-5

Zhang WG, Tang LB, Li HR, Wang L, Cheng LF, Zhou TQ, Chen X (2020b) Probabilistic stability analysis of bazimen landslide with monitored rainfall data and water level fluctuations in three gorges reservoir, china. Front Struct Civ Eng 14:1247–1261. https://doi.org/10.1007/s11709-020-0655-y

Zhang WA, Meng XY, Wang LQ, Meng FS, Wang YK, Liu PF (2023) Reliability evaluation of reservoir bank slopes with weak interlayers considering spatial variability. Front Mar Sci 10. https://doi.org/10.3389/fmars.2023.1161366

Zhang WG, Lin SC, Wang LQ, Wang L, Jiang X, Wang S (2024) A novel creep contact model for rock and its implement in discrete element simulation. Comput Geotech 167. https://doi.org/10.1016/j.compgeo.2023.106054

Zhou C, Yin KL, Cao Y, Ahmed B (2016) Application of time series analysis and pso-svm model in predicting the bazimen landslide in the three gorges reservoir, China. Eng Geol 204:108–120. https://doi.org/10.1016/j.enggeo.2016.02.009

Zhou C, Hu YJ, Xiao T, Ou Q, Wang LQ (2023) Analytical model for reinforcement effect and load transfer of pre-stressed anchor cable with bore deviation. Constr Build Mater 379. https://doi.org/10.1016/j.conbuildmat.2023.131219